PZT-like structural phase transitions in the $BiFeO_3$-$KNbO_3$ solid solution

Robert C. Lennox,[a] Daniel D. Taylor,[b] Laura J. Vera Stimpson[a], Gavin B. G. Stenning,[c] Marek Jura,[c] Mark C. Price,[a] Efrain E. Rodriguez[d] and Donna C. Arnold[a]

[a] School of Physical Sciences, University of Kent, Canterbury, Kent, CT2 7NH, UK

[b] Department of Materials Science and Engineering, University of Maryland, College Park, MD, 20742-2115, USA

[c] ISIS Neutron and Muon Source, Rutherford Appleton Laboratory, Harwell Science and Innovation Campus, Didcot, OX11 0QX, UK

[d] Department of Chemistry and Biochemistry, University of Maryland, College Park, MD 20742-4454, USA

Introduction

The search for new ferroelectric materials is driven by two main themes, namely the hunt for Pb-free ferroelectrics and the renaissance of research in multiferroic materials. $KNbO_3$ (KN) has been widely studied, in combination with $NaNbO_3$, as a Pb-free ferroelectric material.[1] At room temperature KN adopts orthorhombic Amm2 symmetry (Fig. 1) where the ferroelectric character is driven by displacements of the Nb^{5+} ions within the NbO_6 octahedra.[2] $BiFeO_3$ (BFO) on the other hand is by far the most widely studied multiferroic material, primarily due to the observation of room temperature ferroelectric ($T_c \sim 1100$ K) and antiferromagnetic ($T_N \sim 635$ K) ordering.[3] At room temperature, BFO can be described with the Bi^{3+} ions occupying cubo-octahedral positions within the perovskite whilst the Fe^{3+} ions are coordinated in an octahedral arrangement as described by polar R3c symmetry (Fig. 1).[4] In contrast with KN, the ferroelectric character of BFO arises due to the large displacement of the Bi^{3+} ions, as a result of the stereoactive $6s^2$ lone pair of electrons. However, high leakage currents and weak magnetoelectric coupling in BFO are barriers to its commercial use. Researchers have therefore, turned to doping strategies to unwind the complex magnetic spin cycloid and improve the ferroelectric and/or magnetoelectric properties.[4] For example replacing Bi^{3+} on the perovskite A-site with rare earths such as La^{3+} or Nd^{3+} has led to the observation of improved ferroelectric characteristics and the observation of $PbZrO_3$-like antiferroelectric (AFE) order.[5,6]

Given their individual properties, solid-solutions between BFO and KN have unexpectedly received little attention. This is all the more surprising if we consider Goldschmidt tolerance factor arguments. The tolerance factor is related to the ionic radii of the constituent ions as given by the equation below and can be used to describe the distortion in a crystal structure.[7]

$$t = \frac{(r_A + r_o)}{\sqrt{2(r_B + r_o)}}$$

where t is the tolerance factor and r_A, r_B and r_O are the ionic radii of the A, B and oxygen ions respectively. BFO has a tolerance factor of approximately 0.95. If we consider rare earth (RE) doping of BFO this results in a lowering of the tolerance factor, since the ionic radii of RE^{3+} ions are smaller than that of Bi^{3+}.[8] In comparison with the PbZrO3–PbTiO3 (PZT) phase diagram this shifts the tolerance factor towards the Zr^{4+} rich end of the solid solution and the realisation of AFE character as described above. In contrast, doping with KN can be expected to increase the tolerance factor possibly allowing for a structural morphotropic phase boundary (MPB) similar to that observed in PZT to be realised (Fig. 1). This is especially important since it can be expected that *'MPB compositions* similar to PZT can provide clues for the fabrication of lead-free ceramics with *high performance'*.[9] Furthermore the incorporation of magnetic ordering may lead to functional multiferroic materials.

Nakashima et al. prepared materials in the composition range $0 \leq x \leq 0.7$ for $Bi_{1-x}K_xFe_{1-x}Nb_xO_3$ ceramics,[10] they reported that the compositions $Bi_{0.90}K_{0.10}Fe_{0.90}Nb_{0.10}O_3$ and $Bi_{0.80}K_{0.20}Fe_{0.80}Nb_{0.20}O_3$ crystallise with R3c and pseudo-cubic symmetry respectively. In contrast compositions, $x \geq 0.30$ are reported to be cubic. Whilst weak ferroelectric and ferromagnetic character is reported for the $Bi_{0.90}K_{0.10}Fe_{0.90}Nb_{0.10}O_3$ material, high dielectric losses were reported for materials with $x \geq 0.40$.[10] Teslenko et al. investigated materials within the BFO–KN solid solution using X-ray diffraction studies.[11] They later expanded this study to more in-depth characterisation of x = 0, 0.3, 0.5, 0.7 and 1.0 in $Bi_{1-x}K_xFe_{1-x}Nb_xO_3$.[12] These authors postulate that materials between $0 \leq x \leq 0.25$ are characterised with the same polar, R3c symmetry exhibited by the parent BFO material. This is followed by a non-polar, Pbnm → polar, P4mm → polar, Amm2 series of phase transitions at approximately x = 0.55 and 0.85 respectively. At the phase transitions, small regions of phase coexistence are observed. These results would suggest that a PZT-like phase diagram is not obtained for BFO–KN materials. In contrast a rhombohedral → tetragonal phase transition at approximately x = 0.15 has been

reported in the related BFO–$K_{0.5}Na_{0.5}NbO_3$ solid solution with enhanced ferroelectric character observed at x = 0.18.[13]

Clearly the current understanding of this important system is poor. In this communication we report a combined powder neutron diffraction, synchrotron diffraction and Raman spectroscopy study of the BFO-KN solid solution. We see no evidence for the non-polar, Pbnm phase and instead observed a PZT-like R3c → P4mm → Amm2 series of phase transitions making the realisation of a MPB similar to that in PZT an exciting possibility.

Experimental

Materials in the BFO–KN solid solution were synthesised using a similar method to that previously reported by us.[14–16] Stoichiometric ratios of K_2CO_3, Nb_2O_5, Fe_2O_3 and Bi_2O_3 (Sigma Aldrich, ≥99%) were reacted at 800 °C for 5 hours with a 6 mol% excess of both K_2CO_3 and Bi_2O_3 to mitigate against loss of Bi^{3+} and K^+. The resulting powders were leached with 2.5 M HNO_3 under continuous stirring for two hours, washed with ddH_2O and dried for one hour at 400 °C to yield single phase materials. Phase purity was assessed using a Bruker D8 Advance diffractometer equipped with Cu Kα1 radiation (40 kV and 40 mA, λ = 1.540 598 Å) over a two theta range of $10 \leq 2\theta \leq 70$ degrees.

Room temperature powder neutron and synchrotron diffraction measurements were performed on the high resolution powder diffractometer (HRPD) and the high resolution diffraction beamline (I11)[17] at the ISIS facility and Diamond Light Source, UK (λ = 0.825659(2) Å), respectively. Refinements were performed using the general structure analysis system (GSAS) suite of programs.[18,19] X-ray fluorescence spectra were collected using the PANalytical MiniPal4 spectrometer. Raman spectra were collected on a Horiba Yvon Jobin LabRAM instrument at room temperature on powdered samples. SQUID magnetometry measurements were performed on a magnetic property measurement system (MPMS) XL-7 instrument. Dielectric measurements were performed using an Agilent 4294A impedance analyser. All experiments are described in more depth in the ESI.†

Results and discussion

$Bi_{1-x}K_xFe_{1-x}Nb_xO_3$ materials were prepared with compositions between $0 \geq x \geq 1$ with increments of x = 0.05. Powder X-ray diffraction data collected for these materials (not shown) indicated that all materials appeared to be single phase with X-ray fluorescence data indicating the materials were reasonably close to the expected stoichiometries (reported in the ESI†).

Materials with $x \leq 0.10$ exhibit diffraction patterns consistent with R3c symmetry and the parent $BiFeO_3$ material. Between $0.10 \leq x \leq 0.95$ the diffraction patterns suggest the materials exhibit pseudo-cubic symmetry with the x = 1.0 material crystallising with orthorhombic Amm2 symmetry, as expected for KN. These results are consistent with early studies performed on the BFO–KN solid solution and related systems.[10,20,21] In order to understand the pseudo-cubic phase further, we performed more in depth structural studies using powder neutron and synchrotron diffraction experiments. Initial analysis of the synchrotron data indicated a systematic shift in peak position with increasing x (as shown in Fig. 2) consistent with increasing lattice parameters resulting from replacing Bi^{3+} (r = 1.17 Å) with the much larger K^+ (r = 1.51 Å) ion.[8] Both Fe^{3+} and Nb^{5+} have similar ionic radii of 0.645 Å and 0.64 Å, respectively.[8]

Despite repeated attempts we have been unable to refine these data beyond x = 0.15 (reported in the ESI†) primarily due to the broad anisotropic peak profiles exhibited by these materials. Refinements typically failed to adequately model either the peak shape and/or peak intensity. In order to try and overcome these issues we considered peak shape initially considering a pseudo-Voigt function (profile function type 2 in the GSAS suite of programs) as described by Howard and Thompson et al.[22,23] and various symmetries including R3c, R3m, P4mm, Amm2 and $Pm\bar{3}m$ including two phase mixtures. We further expanded these refinements to consider compositional variations across crystallites using the Stephen's micro strain broadening model (profile function type 4 in the GSAS suite of programs).[16,22–27] In all cases the refinements proved unstable and still failed to accurately model our data. In order to simplify these refinements, we performed Le Bail refinements with our data.[28] This method allows us to evaluate our models by investigating the 'best fit' achievable without taking into account structural parameters and permitting peak shape and lattice parameters to be fit. Whilst this vastly improved our refinements, these still proved to be far from ideal. These data strongly suggest that these materials are fairly inhomogeneous in nature exhibiting complex diffraction patterns made up of multiple phases with multiple lattice parameters. Using the Le Bail method, however, we were able to note, on average, a preliminary series of phase transitions for materials between $0.15 \leq x \leq 0.95$. Between $0.15 \leq x \leq 0.35$ materials exhibit a mixture of phases with R3c and P4mm symmetries. Pseudo-single phase P4mm symmetry is observed between x = 0.40 and 0.55. Above x = 0.55 a mixture of phases with P4mm and Amm2 symmetries is observed.

In contrast to our X-ray data analysis, we were able to model our powder neutron diffraction data more successfully as shown in the ESI.† Refinements, suggest a R3c → P4mm → Amm2

series of phase transitions consistent with our synchrotron diffraction analysis. We note that high thermal parameters are observed, particularly for the Bi^{3+}/K^{+} crystallographic A-site This suggests that our samples are probably comprised of regions with different Bi^{3+}:K^{+} and Fe^{3+}:Nb^{5+} ratios and thus compositions with a distribution of lattice parameters consistent with the broad peaks exhibited in both our neutron and synchrotron data. Furthermore, close inspection of the refinement data demonstrates some evidence of un-indexed peaks, which are attributable to small amounts of secondary phases in some materials and the possible persistence of magnetic Bragg and/or superstructure peaks at low values of x warranting further investigation.

In order to compare the trends in the lattice parameters and cell volume across the entire composition range we related our lattice parameters to the aristotype cubic perovskite geometry. For P4mm the relationship is straightforward with a $a_{tet} = a_{cub}$, and $c_{tet} = a_{cub}$ setting; for Amm2 the lattice parameters can be related through a $a_{orth} = a_{cub}$, $b_{orth} = \sqrt{2}a_{cub}$ and $c_{orth} = \sqrt{2}a_{cub}$ relationship. It can be seen that the cell volume increases with increasing x as expected from differences in the ionic radii as described above. A clear change in slope is evident at approximately x = 0.7 consistent with the phase transition between P4mm and Amm2 symmetry as shown in Fig. 3. The lattice parameters, however, show a more complex and interesting trend (Fig. 3b). In the P4mm phase, the lattice parameters, a, b and c all increase linearly up to x = 0.6 before dropping slightly at x = 0.7 as the transition between P4mm and Amm2 symmetries is approached. Whilst the a parameter continues to increase with increasing x, the b parameter changes very little with the c parameter dropping to be more consistent with the b parameter. P4mm symmetry can be described by an order parameter (0, 0, a) with the atomic displacements lying along the [001] direction from the cubic perovskite. [2,29] In contrast Amm2 symmetry is described by an order parameter (a, a, 0) with the atomic displacements lying along the [011] direction.[2,29] This increased tilting of the octahedra coupled with the rotation of displacements leads to the complex behaviour observed in the lattice parameters.

Also notable is the growing 'tetragonality' observed in the P4mm phase with increasing x. In comparison with the almost cubic lattice parameters observed at x = 0.20, the difference between a and c is larger for x = 0.70 (Fig. 3b). If we consider the bond lengths, P4mm symmetry can be described by four equal equatorial bond lengths which sit in the ab plane and two unequal apical bond lengths in the c direction, which represent the displacement of the metal cation within the octahedra. Below x = 0.4 there is only a small difference between the apical bond lengths representing a small displacement on the metal cation as shown in Fig. 3c

and the ESI.† As x increases these bond lengths clearly separate to give one short and one long M–O bond with increasing displacement of the metal cation within the octahedra. Given the pseudo-cubic nature of materials with $x \leq 0.4$ we considered the possibility of alternative symmetries. The work by Teslenko et al. suggests that the transition from R3c to P4mm symmetry occurs through an intermediary non-polar Pbnm phase.[11,12] We find no evidence for a possible Pbnm phase in any of our data either as a primary or secondary phase.

More recently, doping a related rhombohedral (R3c) perovskite, $Bi(Fe_{2/8}Mg_{3/8}Ti_{3/8})O_3$, with $BaTiO_3$ has been shown to reduce the rhombohedral distortion resulting in a phase transition to pseudo-cubic R3m symmetry.[30] This is driven by the larger Ba^{2+} cation substituting for the smaller Bi^{3+} cation on the perovskite A-site, which suppresses the tilting of the BO_6 octahedra. Similarly, since the ionic radii of K^+ is much larger than Bi^{3+}, the possibility of a R3c → R3m phase transition in our materials was also considered. Refinements of the x = 0.20 material with and R3m model did not lead to a statistical improvement of the refinement. Since our smallest value of x is 0.2 for our powder neutron diffraction study, we cannot rule out that this transition occurs at $x \leq 0.2$ and this warrants further investigation.

From our current study we propose a phase diagram similar to that observed for the $PbZrO_3$–$PbTiO_3$ solid solution as shown in Fig. 4. We note large regions of phase coexistence are observed most likely due to the inhomogeneous nature of our materials. Sharper phase transitions may be realised through optimisation of the synthesis methodologies similar to those used to improve the homogeneity in other $BiFeO_3$ based materials such as that reported for Nd^{3+} doped $BiFeO_3$.[5]

In order to further investigate the symmetry considerations in these materials we performed room temperature Raman spectroscopy as described in the ESI.† As expected sharp peaks are observed for both the $BiFeO_3$ and $KNbO_3$ end members. The assignment of phonon modes for these materials has been discussed at length elsewhere and will not be presented here.[16,31–33] In contrast broad peaks are observed for materials in the composition range $0.1 \leq x \leq 0.9$ due to the largely inhomogeneous nature of these materials.† We note that care needs to be taken when assigning symmetry to point spectra from powdered samples due to the inhomogeneous nature of the samples. In addition, the expected polar nature of these materials further complicates analyses of the Raman spectra collected as a result of the random orientation of grains which can lead to phonon modes that vary in both intensity and position. [4] It is therefore

not possible to extract any meaningful conclusions from small peak shifts in our Raman data. However, close analysis of the overall profile of our spectra can provide information to support structural phase transitions in these materials. At $x = 0.10$ the spectra is strikingly similar to that collected for the parent $BiFeO_3$ material suggesting that on average this material exhibits R3c symmetry as expected. Likewise for materials with compositions of $x \geq 0.80$ the spectra are in line with that of $KNbO_3$, which suggests that these materials exhibit Amm2 symmetry. In the composition range $0.20 \leq x \leq 0.6$ the spectra are characterised by the presence of 3 peaks which suggests that these materials exhibit a single symmetry that is neither R3c nor Amm2. Indeed, this observation suggests P4mm symmetry for this composition range as evidenced by the powder neutron diffraction data discussed above. Surprisingly the spectra collected for the $Bi_{0.30}K_{0.70}Fe_{0.30}Nb_{0.70}O_3$ material resembles that of Amm2 and is most likely due to phase segregation. As with our diffraction studies, we found no evidence in the Raman spectra for the Pbnm phase reported by Teslenko et al.[11,12]

Preliminary magnetic and electrical data exhibit some interesting behaviour yet confirm the inhomogeneous nature of the samples. Variable temperature zero-field cooled (ZFC) and field cooled (FC) data collected for materials with $x \geq 0.5$ (given in the ESI†) showed curves consistent with paramagnetic behaviour. A small deviation was seen between ZFC and FC data at approximately 15 K. Curie–Weiss fits to the paramagnetic region (between 200 and 300 K) gave negative Weiss constants, θ, suggestive of either spin glass or canted antiferromagnetic (AFM) behaviour. A slight deviation from linearity is also observed in magnetisation-field curves at 25 K in these materials (see ESI†). The most likely origin of this behaviour is the formation of Fe^{3+} rich regions in the material, consistent with our observations of the inhomogeneous nature of these materials, or possibly small amounts of Fe based impurities not detectable by diffraction techniques. At $x = 0.4$ there is no evidence for any hysteretic behaviour either at 25 K or 300 K. However, a deviation between the ZFC-FC data is observed at approximately 50 K indicative of a spin glass transition. For materials with $x \leq 0.3$ non Curie–Weiss like behaviour is observed across the entire temperature range studied (2 K– 300 K). Instead, we observed a broad peak that straddles up to room temperature coupled with a glassy-like transition at approximately 50 K, consistent with that observed for the $Bi_{0.6}K_{0.4}Fe_{0.6}Nb_{0.4}O_3$ materials. This would suggest the possibility of a low dimensional AFM transition in these materials close to room temperature.

In contrast with RE^{3+} doped materials the magnetization measurements suggest that increasing x leads to a lowering of the AFM transition due to the decreasing amounts of Fe^{3+} in the materials. Furthermore, weak hysteresis at 25 K and 300 K in these materials also supports the observation of an above or close to room temperature transition and suggests canted AFM behaviour due to the unwinding or disruption of the magnetic spin cycloid. In all cases the hysteresis loops do not fully saturate. Previously in rare earth doped materials, this lack of saturation has been suggested to be related to the magnetisation effects of the paramagnetic RE^{3+} ion on the iron sublattice.[16,34] However, in these materials it is more likely that the addition of ions to both the A- and B-site lattices disrupts the long range ordering. It is also not clear from these data if they exhibit a paramagnetic – antiferromagnetic – spin glass series of transitions as has been previously suggested for $BiFeO_3$[3] or if these behaviour are linked with Fe^{3+} rich and Fe^{3+} deficient areas arising due to sample inhomogeneities.

Electrical measurements were performed for x = 0.1, 0.2, 0.3, 0.4, 0.5 and 0.8 materials. In all cases the materials exhibited high permittivity frequency dependent behaviour typical of non-ohmic electrode effects arising from 'leaky' dielectric behaviour (as shown in the ESI†).[16,35,36] It was not possible to collect polarisation-field data as a result of the 'leaky' nature of these materials. With the exception of the x = 0.5 material all samples show some anomalies in the dielectric constant between 500 and 700 K coupled with anomalies close to room temperature. Whilst this is interesting it is impossible to extract anything meaningful from these data and therefore difficult to confirm the polar nature of these materials. However, these results clearly suggest the possibility of exciting electrical behaviour in these materials and more in-depth studies on homogenous samples are required to fully understand these behaviour.[5]

Conclusions

In summary we report a comprehensive structural study of materials in the $BiFeO_3$–$KNbO_3$ solid solution using powder neutron diffraction and complimentary Raman spectroscopy. In contrast with previous reports, we propose a R3c → P4mm → Amm2 series of phase transitions. Materials with compositions of $x \leq 0.1$ and $x \geq 0.7$ adopt the $BiFeO_3$, R3c and $KNbO_3$, Amm2 symmetries respectively. In contrast in the composition range $0.5 \leq x \leq 0.6$ materials with P4mm symmetry are obtained. Analysis of the current data suggests that the $Bi_{0.30}K_{0.70}Fe_{0.30}Nb_{0.70}O_3$ material exhibits the largest displacement of the BO_6 octahedra. Furthermore, the pseudo-cubic nature of materials with small values of x may suggest that an

R3c → R3m → P4mm → Amm2 series of phase transitions is perhaps more appropriate and this warrants further investigation.

Interestingly, the proposed phase diagram strikingly resembles that exhibited by the important $PbZrO_3$–$PbTiO_3$ solid solution. Therefore, the realisation of materials close to MPB similar to that in PZT with the potential to exhibit enhanced properties is an exciting possibility. Furthermore, preliminary magnetic and electrical measurements, whilst inconclusive in the current study, suggest the enticing opportunity for the synthesis of high performance multiferroic materials.

Acknowledgements

DCA and RCL would like to thank the South East Physics Network (SEPnet) for the provision of a PhD studentship. RCL would like to thank Dr Nikitas Gidopoulos. EEF and DDT acknowledge the University of Maryland's X-ray Crystallography Center and the University's support from start-up funds. We thank the STFC for facilities access and the Diamond Light Source and the ISIS neutron source for access to I11 (EE9194) and HRPD (RB1220271) beamlines respectively. We would also like to thank Dr Claire Murray, Dr Chui Tang and Dr Aziz Daoud-Aladine for assistance conducting these experiments. DCA would also like to thank Dr Finlay Morrison for access to impedance spectroscopy, Professor Igor Levin and Dr Emma McCabe for useful discussion, and Mr William Jamieson and Miss Michaela Regan for their contributions to this work.

References

1 T. R. Shrout and S. J. Zhang, J. Electroceram., 2007, 19, 11345.

2 A.W.Hewat, J. Phys. C: Solid State Phys., 1973, 6, 2559.

3 G. Catalan and J. F. Scott, Adv. Mater., 2009, 21, 2463.

4 D. C. Arnold, IEEE Transactions on Ultrasonics, Ferroelectrics and Frequency Control, 2015, 62, 62.

5 I. Levin, M. G. Tucker, H. Wu, V. Provenzano, C. L. Dennis, S. Karimi, T. Comyn, T. Stevenson, R. I. Smith and I. M. Reaney, Chem. Mater., 2011, 23, 2166.

6 D. A. Rusakov, A. M. Abakumov, K. Yamaura, A. A. Belik, G. Van Tendeloo and E. Takayama-Muromachi, Chem. Mater., 2011, 23, 285.

7 V. M. Goldschmidt, Naturwissenschaften, 1926, 14, 477.

8 R. D. Shannon, Acta Crystallogr., Sect. A: Cryst. Phys., Diffr., Theor. Gen. Cryst., 1976, 32, 751.

9 E. Magome, Y. Kuroiwa, H. Yoshimura, C. Moriyoshi, K. Yamashita, I. Fujii, K. Nakashima, N. Kumada and S. Wada, Jpn. J. Appl. Phys., 2012, 51, 0905.
10 Y. Nakashima, T. Shimura, W. Sakamoto and T. Yogo, Ferroelectrics, 2007, 356, 180.
11 P. Y. Teslenko, Y. V. Kabirov, O. N. Razumovskaya and L. A. Reznichenko, Bull. Russ. Acad. Sci.: Phys., 2011, 75, 1133.
12 P. Y. Teslenko, A. G. Razumnaya, V. O. Ponomarenko, A. G. Rudskaya, A. V. Nazarenko, A. S. Anokhin, M. V. Avramenko, D. I. Leshov, M. F. Kupriyanov and Y. I. Yuzyuk, Phys. Solid State, 2014, 56, 1866.
13 S. X. Huo, S. L. Yuan, Y. Qiu, Z. Z. Ma and C. H. Wang, Mater. Lett., 2012, 68, 8.
14 D. C. Arnold, K. S. Knight, F. D. Morrison and P. Lightfoot, Phys. Rev. Lett., 2009, 102, 027602.
15 D. C. Arnold, K. S. Knight, G. Catalan, S. A. T. Redfern, J. F. Scott, P. Lightfoot and F. D. Morrison, Adv. Funct. Mater., 2010, 20, 2116.
16 R. C. Lennox, M. C. Price, W. Jamieson, M. Jura, A. Daoud- Aladine, C. Murray, C. Tang and D. C. Arnold, J. Mater. Chem. C, 2014, 2, 3345.
17 S. P. Thompson, J. E. Parker, J. Potter, T. P. Hill, T. M. Cobb, F. Yuan and C. C. Tang, Rev. Sci. Instrum., 2009, 80, 075107.
18 A. C. Larson and R. B. V. Dreele, Los Alamos National Laboratory Report LAUR, 1994, 96, 86.
19 B. H. Toby, J. Appl. Crystallogr., 2001, 34, 210.
20 X. Chao, Z. Yang, Z. Li and Y. Li, J. Alloys Compd., 2012, 518, 1.
21 Y. Ma and X. M. Chen, J. Appl. Phys., 2009, 105, 054107.
22 C. J. Howard, J. Appl. Crystallogr., 1982, 15, 615.
23 P. Thompson, D. E. Cox and J. B. Hastings, J. Appl. Crystallogr., 1987, 20, 79.
24 B. van Laar and W. B. Yelon, J. Appl. Crystallogr., 1984, 17, 47.
25 L. W. Finger, D. E. Cox and A. P. Jephcoat, J. Appl. Crystallogr., 1994, 27, 892.
26 P. Stephens, J. Appl. Crystallogr., 1999, 32, 281.
27 A. Leineweber and E. J. Mittemeijer, J. Appl. Crystallogr., 2004, 37, 123.
28 A. Le Bail, H. Duroy and J. J. Fourquet, Mater. Res. Bull., 1988, 23, 447.
29 C. J. Howard and H. T. Stokes, Acta Crystallogr., Sect. A: Fundam. Crystallogr., 2005, 61, 93.
30 M. Dolgos, U. Adem, X. Wan, Z. Xu, A. J. Bell, T. P. Comyn, T. Stevenson, J. Bennett, J. B. Claridge and M. J. Rosseinsky, Chem. Sci., 2012, 3, 1426.

31 J. Bielecki, P. Svedlindh, D. T. Tibebu, S. Cai, S.-G. Eriksson, L. Borjesson and C. S. Knee, Phys. Rev. B: Condens. Matter Phys., 2012, 86, 184422.

32 J. Hlinka, J. Porkorny, S. Karimi and I. M. Reaney, Phys. Rev. B: Condens. Matter Phys., 2011, 83, 020101.

33 Z. X. Shen, Z. P. Hu, T. C. Chong, C. Y. Beh, S. H. Tang and M. H. Kuok, Phys. Rev. B: Condens. Matter Phys., 1995, 52, 3976.

34 V. A. Khomchenko, D. V. Karpinsky, A. L. Kholkin, N. A. Sobolev, G. N. Kakazei, J. P. Araujo, I. O. Troyanchuk, B. F. O. Costa and J. A. Paixao, J. Appl. Phys., 2010, 108, 074109.

35 M. Li, A. Feteira and D. C. Sinclair, J. Appl. Phys., 2009, 105, 114109.

36 M. Li, D. C. Sinclair and A. R. West, J. Appl. Phys., 2011, 109, 084106.

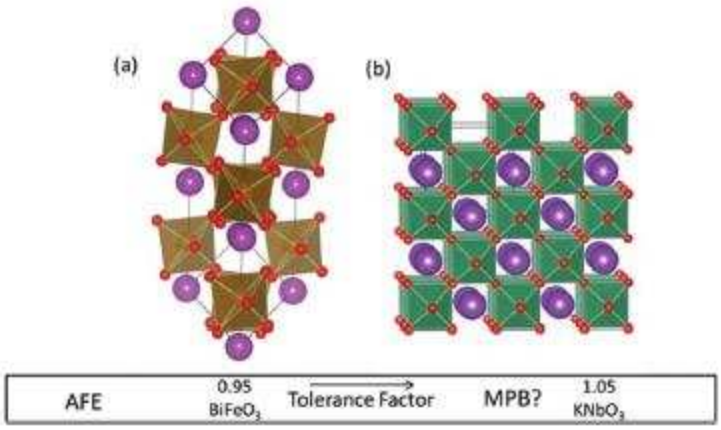

Fig. 1 Schematic representation of (a) $BiFeO_3$ in the hexagonal setting of the R3c space group where the brown squares represent the FeO_6 octahedra, the purple spheres represent the Bi^{3+} ions and the red spheres represent the oxygen ions respectively, (b) orthorhombic Amm2, $KNbO_3$ where the green squares represent the NbO_6 octahedra, the purple spheres represent the K^+ ions and the red spheres represent the oxygen ions respectively and phase diagram showing the relationship with tolerance factor, t, with the PZT phase diagram showing the regions of antiferroelectric (AFE) behaviour and the potential for morphotropic phase boundaries (MPB) with decreasing and increasing t respectively.

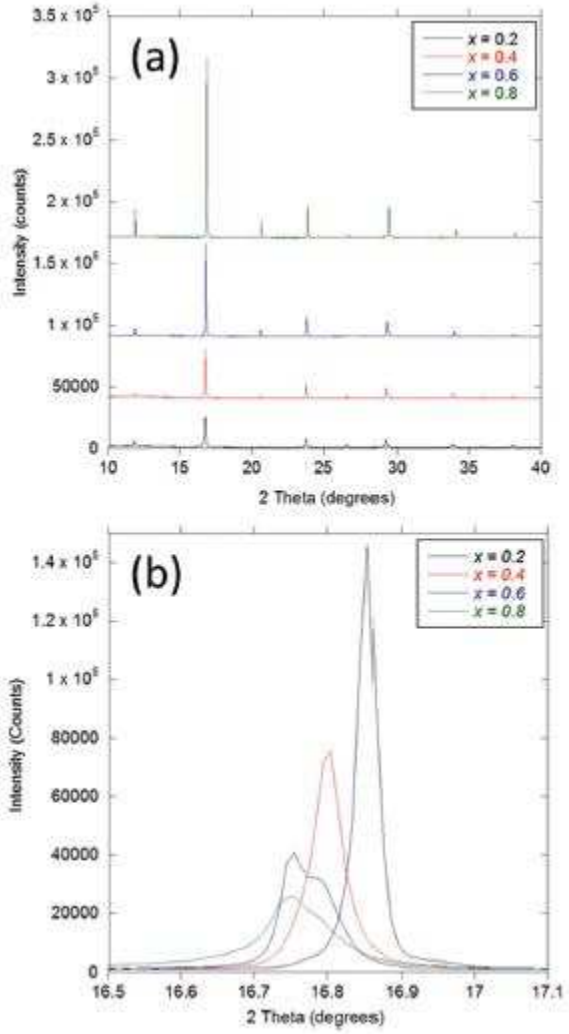

Fig. 2 (a) and (b) Synchrotron diffraction patterns collected for Bi_{1-x}- $K_xFe_{1-x}Nb_xO_3$ materials with x = 0.2, 0.4, 0.6 and 0.8 showing the shift in peak position and thus lattice parameters with increasing values of x.

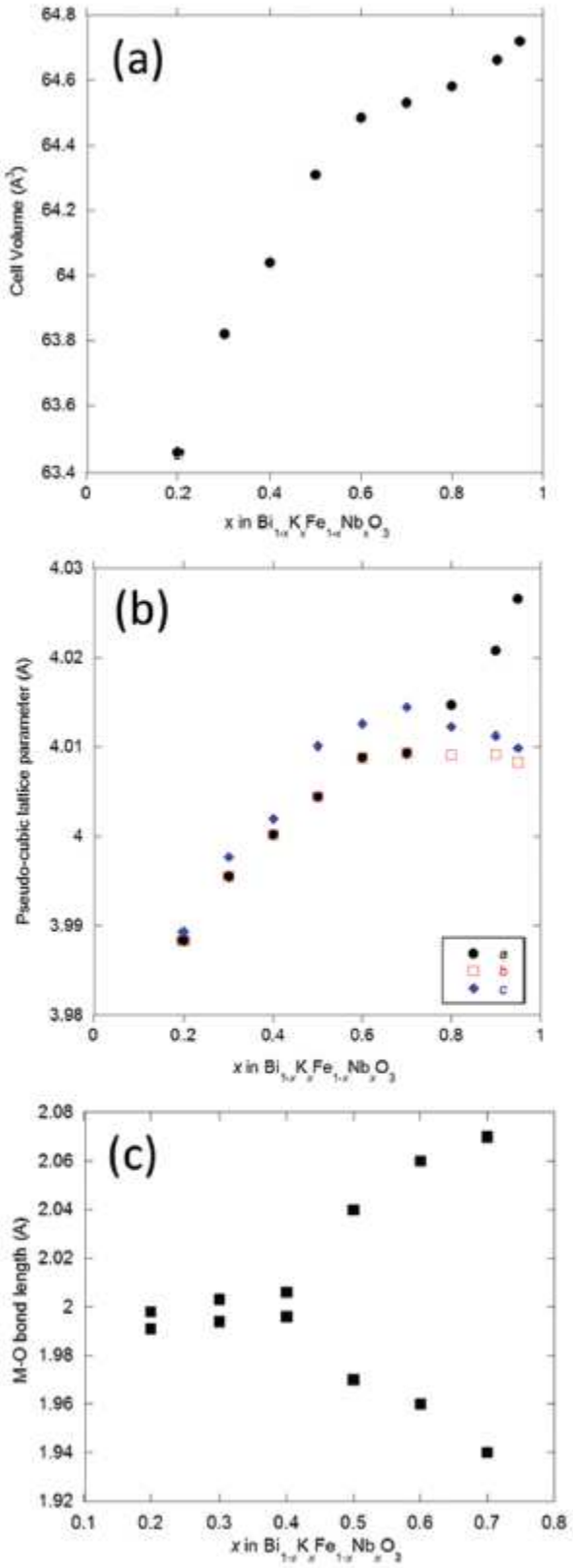

Fig. 3 Neutron powder diffraction results for (a) pseudo-cubic cell volume, (b) pseudo-cubic lattice parameters and (c) apical Fe/Nb–O bond length as a function of x in $Bi_{1-x}K_xFe_{1-x}Nb_xO_3$ materials (note: error bars are smaller than the symbol size. Error values are given in the ESI†).

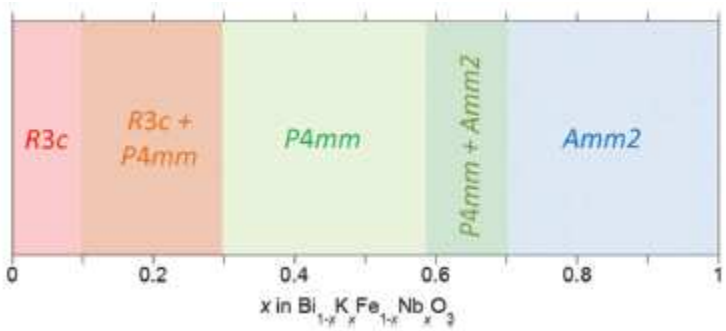

Fig. 4 Proposed phase diagram for $Bi_{1-x}K_xFe_{1-x}Nb_xO_3$ materials based on powder diffraction studies.